Food Chemistry: X 21 (2024) 101149

Contents lists available at ScienceDirect

Food Chemistry: X

journal homepage: www.sciencedirect.com/journal/food-chemistry-x

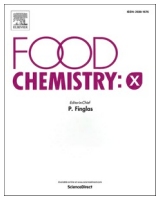

Simultaneous ultrasound and microwave application in myosin-chlorogenic acid conjugation: Unlocking enhanced emulsion stability

Zhiyu Li [a,1], Xiaomei Zhong [b,1], Cuirong Luan [a], Nanhua Wen [a], Chuanyang Shi [c], Shuji Liu [d], Yizhou Xu [b], Quan He [e], Yijing Wu [a,f,*], Jie Yang [a,f,*]

[a] Institute of Oceanography, Department of Geography and Oceanography, Minjiang University, Fuzhou, China
[b] College of Oceanography, Fujian Agriculture and Forest University, Fuzhou, China
[c] Department of Nutrition and Food Studies, Steinhardt School of Culture, Education, and Human Development, New York University, NY, United States
[d] Key Laboratory of Cultivation and High-value Utilization of Marine Organisms in Fujian Province, Fisheries Research Institute of Fujian, Xiamen, China
[e] Department of Engineering, Faculty of Agriculture, Dalhousie University, NS, Canada
[f] Fujian Key Laboratory on Conservation and Sustainable Utilization of Marine Biodiversity, Minjiang University, Fuzhou, China

ARTICLE INFO

Keywords:
Myosin
Conjugation
Combined ultrasound-microwave treatment
Emulsifying behavior
Stability

ABSTRACT

This study investigated the grafting chlorogenic acid (CA) onto myosin, utilizing various techniques including conventional method, ultrasound, microwave, and combination of ultrasound and microwave (UM). The grafting efficiency was as follows: conventional method < microwave < ultrasound < UM. The UM technique manifested the highest CA-binding capacity (80.26 μmol/g myosin) through covalent bonding, and a much shorter time was required for conjugation than conventional method. The conjugation of polyphenol significantly increased the solubility of myosin with reduced aggregation behavior, which was accompanied by structural alterations from ordered structures (α-helix and β-sheet) to disordered forms. The emulsion stabilized by UM-myosin-CA conjugate exhibited the most homogeneous microstructure with favorable creaming stability. Moreover, the resulting emulsion presented strong oxidation resistance and storage stability. These results illustrate the promising potential of employing CA-grafted myosin, especially when processed using the UM technique, in the development of highly efficient emulsifiers.

1. Introduction

At present, there is growing interest in the development of products containing polyunsaturated fatty acids (PUFAs) across the food and pharmaceutical sectors (Ji & Ledesma-Amaro, 2020; Tang et al., 2023). Numerous studies have proved the health-promoting effects of PUFAs, including blood pressure regulation, anti-inflammatory properties, and facilitation of neurological development (Hauser et al., 2018). To maximize these functionalities, PUFAs are commonly incorporated into emulsified food products. However, emulsions containing PUFAs are intrinsically susceptible to various forms of environmental stress, especially for oxidative conditions (Lv et al., 2023). In particular, the presence of double bonds within PUFAs renders them vulnerable to oxidation, resulting in the formation of saturated aldehydes. These oxidation products adversely impact the nutritional values (Franklin et al., 2017; Xue et al., 2023). Therefore, there exists a profound necessity in the design and development of functional emulsifiers capable of mitigating the oxidative degradation of PUFAs within emulsion systems.

Myosin, a main component of meat products, is considered as the promising food ingredient due to its high biocompatibility and multifunctionality (Zhu et al., 2022). However, myosin is prone to self-associate into rod-like multimer structures, and the hydrophobic amino acid residues are inherently buried within the interior of protein. Both of these limited its stability in oil–water interfaces, which reduces the effectiveness of myosin as an emulsifier (Huang et al., 2021). Therefore, there is a pressing need to engineer myosin-based emulsifiers that not only exhibit advanced emulsification properties but also demonstrate antioxidative functionalities. Covalently bonded conjugates of proteins and polyphenols have been identified as promising candidates for emulsifiers with both advanced emulsifying and antioxidative capacities (Liu et al., 2023). Specifically, the covalent grafting

* Corresponding authors at: Institute of Oceanography, Department of Geography and Oceanography, Minjiang University, Fuzhou, China.
E-mail addresses: yijingwu@mju.edu.cn (Y. Wu), jie.yang@mju.edu.cn (J. Yang).
[1] These authors contributed to this work equally.

https://doi.org/10.1016/j.fochx.2024.101149
Received 19 November 2023; Received in revised form 4 January 2024; Accepted 16 January 2024
Available online 20 January 2024

of polyphenols onto proteins can effectively modify the structural properties of polypeptides, making it more amenable for interfacial activity (Wang et al., 2024). Simultaneously, the inherent antioxidative characteristics of polyphenols serve to attenuate the formation of hydroperoxides, contributing to neutralizing reactive oxygen species (Liu et al., 2023). Previous studies have also confirmed that covalent protein–polyphenol conjugates display more pronounced effects than that of non-covalently bonded complexes in terms of the emulsifying behaviors and oxidation resistance (Baba et al., 2021; Wei et al., 2015).

Nonetheless, conventional method of fabricating covalent protein–polyphenol conjugates is featured with low-efficiency. Ultrasound technology, which is efficient, safe, and environmentally friendly, has been extensively employed to accelerate the grafting process (Sun et al., 2022). Ultrasonic cavitation is capable of modifying both globular and fibrous proteins by disrupting inter- and intra-molecular forces, thereby exposing active sites for the grafting reaction (Iscimen et al., 2023). Furthermore, local translational motions induced by continuous acoustic streaming and micro-jetting facilitate the close proximity of protein and polyphenol, thereby establishing a more stable reaction environment (Yan et al., 2023). However, ultrasound penetration is limited in highly aggregated structures, as elucidated in our prior research (Li et al., 2020). Hence, there is pressing need for the development of a methodology that can avoid the adverse effect inherent in standalone ultrasound-based approach while concurrently improving grafting efficiencies.

The utilization of microwave technology in the fabrication of protein-based conjugates represents an emergent area of research (Nasrollahzadeh et al., 2017). This technique leverages electromagnetic fields to accelerate the kinetics of interactions between proteins and polyphenols. However, the uncontrolled heating effects associated with microwave application may compromise the functional properties of the resultant conjugates (Sun et al., 2020). Consequently, despite the promising capabilities of both ultrasound and microwave technologies, their intrinsic limitations restrict their broad applicability in the field of food engineering. The simultaneous use of ultrasound and microwave (UM) technologies has been reported in various applications, such as the extraction of bioactive compounds and biodiesel production, where synergistic effects have been observed (Kodgire et al., 2023; Yadav et al., 2023). To the best of our knowledge, the UM technique has yet to be applied to the synthesis of protein–polyphenol conjugates. As such, it remains undetermined whether UM-facilitated conjugation leads to higher conjugation yield compared to the conventional method, microwave, and ultrasound alone. Additionally, further research is warranted to ascertain whether conjugates synthesized via UM method demonstrates enhanced emulsifying properties, particularly under varying environmental stress conditions.

The present study aims to enhance the emulsifying capabilities of myosin by grafting it with polyphenol, specifically chlorogenic acid (CA), which is a class of naturally occurring compounds with antioxidant properties and can be commonly found in a variety of plants (Pan et al., 2022). Various techniques including conventional method, microwave, ultrasound, and UM approach were employed to assist the grafting process. The impact of these different grafting methods on the structural properties of the resultant conjugates were assessed through measurements of total CA content, molecular weight, and spectroscopic analyses. Additionally, the study also investigated the aggregation behaviors and antioxidant activity of the synthesized conjugates. The emulsifying properties of the various conjugates were evaluated by characterizing the microstructure of freshly prepared oil-in-water (O/W) emulsions, subsequently, their storage, creaming, and oxidation stabilities were completely assessed. The findings from this investigation are anticipated to expand the applications of UM technique in the development of functional foods and to illustrate the promising potential of CA-grafted myosin for the formulation of highly stable and value-added emulsions.

2. Materials and methods

2.1. Materials

Golden threadfin bream (1–1.5 kg) was supplied by Tengxin Foods Co., Ltd. (FuZhou, China). Subsequent to the removal of viscera and adipose tissue, the muscular tissue was isolated from the skin and skeletal framework. The isolated muscle tissue was refrigerated at 4 °C and utilized for myofibrillar protein extraction within a 6-hour window. CA was purchased from Macklin Biochemical Technology Co., Ltd. (Shanghai, China). All reagents employed in this investigation were of analytical grade and used as received.

2.2. Myosin extraction

In brief, fish muscle (100 g) was homogenized by blending it with 1 L Extract A (0.10 mol/L KCl and 20.00 mmol/L Tris-HCl at a pH of 7.50). The resulting mixture underwent centrifugation at 7155×*g* for 10 min at a temperature of 4 °C to yield a precipitate. Subsequent to supernatant removal, the precipitate was re-homogenized with 50 mL Extract B (0.45 mol/L KCl, 20.00 mmol/L Tris-HCl, 0.20 mol/L Mg $(COO)_2$, 1.00 mmol/L ethylene glycol-bis(2-aminoethylether)-tetraacetic acid (EGTA), and 5.00 mmol/L β-mercaptoethanol (β-ME) at a pH of 6.80). The homogenate was allowed to incubate for 90 min prior to another centrifugation under identical conditions to acquire the supernatant.

The obtained supernatant was combined with 200 mL of 1 mol/L $KHCO_3$ and permitted to react for 20 min, followed by centrifugation at 7155×*g* for 20 min. The resultant precipitate was subjected to homogenization with a 160 mL Extract C (0.50 mol/L KCl, 20.00 mmol/L Tris-HCl, and 5.00 mmol/L β-ME at a pH of 7.50) and allowed to react for an additional 15 min. A 560 mL Extract D (0.50 mol/L KCl, 20.00 mmol/L Tris-HCl at a pH of 7) was subsequently introduced, thoroughly mixed, and left to incubate overnight. The solution was then centrifuged at 7155×*g* for 15 min to collect the precipitate, that is myosin. The entire extraction procedure was rigorously conducted at a temperature of 4 °C. The isolated myosin was solubilized in a buffer containing 20.00 mmol/L Tris-HCl and 0.6 mol/L NaCl at a pH of 7.40, and its concentration was determined via the biuret assay. The myosin sample was kept at 4 °C and used within 4 h.

2.3. Fabricating the myosin-CA conjugate

2.3.1. Ultrasound-assisted conjugation

In order to obtain covalent complexation between CA and myosin, the pH was adjusted to 9.0 using 0.5 M NaOH after 100 mL myosin (10 mg/mL) and CA (1 mg/mL) solutions were mixed. An XH300B ultrasound-microwave (UM) reactor (Beijing Xianghu Science and Technology Development Co. Ltd., China) equipped with a cooling-water-circulating device was used to induce an ultrasound-assisted conjugation, and the treating process was controlled by a UM station (Model OSR-8, Fiso, Canada). Before reaction, the protein–polyphenol mixture was quickly loaded into a four-necked flask. Ultrasonic treatment was carried out at 28 kHz at 100 W until the temperature was 50 °C, and was maintained at 50 °C for 30 min in the ultrasound field. The temperature was allowed to fluctuate by ±1.5 °C during the procedure. After treatment, 0.5 M HCl was applied to adjust pH of the solution to 7.0, and then a dialysis bag with a molecular weight cut-off of 5000 Da was placed in the distilled water to remove any unbound polyphenols for 48 h at 4 °C. The treated myosin was designated U-myosin-CA, which was freeze-dried into powder for further usage within 1 week.

2.3.2. Microwave-assisted conjugation

A microwave-assisted conjugation was performed as described above for ultrasound-assisted samples, except the mixture was microwaved at 100 W until the temperature reached 50 °C, and subsequently

maintained at 50 °C for 30 min under a 2.45 kHz microwave field. The ultrasonic probe was switched off during the microwave-treated procedure. After treatment, the pH of solution was adjusted to 7.0, and then a dialysis bag with a molecular weight cut-off of 5000 Da was placed in the distilled water to remove any unbound polyphenols for 48 h at 4 °C. The treated myosin was designated M-myosin-CA, which was freeze-dried into powder for further usage within 1 week.

2.3.3. Combined UM-assisted conjugation

Both microwave and ultrasound sources were applied in this process. The frequencies of the ultrasound and microwaves were set to 28 kHz and 2.45 kHz, respectively. Combined UM-assisted conjugation was performed as described above for ultrasound-assisted and microwave-assisted samples, except the mixture was treated with simultaneously 100 W microwave power coupled with 100 W ultrasonic power until the temperature was 50 °C, and subsequently maintained at 50 °C for 30 min under the combined UM field. This sample are referred to as UM-myosin-CA. The same myosin and CA mixtures were treated by conventional method alone at 50 °C for 12 h as the control groups, which was referred to as C-myosin-CA. The powders were obtained by following the identical procedures with ultrasound and microwave treatment and utilized within 1 week as well.

2.4. Determination of CA binding capacity

The quantification of total phenolic content was measured utilizing the Folin-Ciocalteau method, with chlorogenic acid (CA) serving as the standard reference (Zheng et al., 2023). An aliquot of 0.5 mL of the conjugate sample was mixed with 2.5 mL of 0.2 N Folin-phenol reagent and vigorously agitated. The reaction mixture was incubated at ambient temperature for a duration of 30 min, shielded from exposure to light. A sodium carbonate solution was subsequently introduced into the reaction mixture, which was further incubated for 2 h, also at ambient temperature and devoid of light exposure. Spectrophotometric analysis was carried out at a wavelength of 760 nm to determine the absorbance, from which the binding content of CA was extrapolated based on the CA standard curve.

2.5. SDS-PAGE

Sodium Dodecyl Sulfate-Polyacrylamide Gel Electrophoresis (SDS–PAGE) was utilized to analyze the molecular weight distributions of conjugate samples, based on the methodology delineated by Zheng et al. (2023). An equal proportion of 0.4 % (w/v) sample solution and Tris-HCl buffer (4 % w/v SDS; 20 % v/v glycerol; 10 % 2-mercaptoethanol; 0.004 % w/v bromophenol blue; pH 6.8) was mixed, followed by heating for 5 min at 100 °C and then quickly cooled to room temperature. 5 % (v/v) stacking gel and 12 % (v/v) separating gel were prepared and 10 μL of each sample solution was loaded into each lane. The electrophoresis was carried out under a constant voltage of 80 V at room temperature. The protein in gel sheet was stained by bromophenol blue for 120 min.

2.6. Solubility

Protein solubility was quantified utilizing the Biuret assay. Protein specimens were formulated to achieve a concentration of 0.4 % (w/v), with the pH normalized to 7.5. Following centrifugation at 4000×*g* for 15 min at a temperature of 4 °C, the supernatant was isolated. A volume of 200 μL of this supernatant was then mixed with 1 mL of Biuret reagent and subjected to a one-hour incubation period. Absorbance was assessed at a wavelength of 540 nm employing a Lambda 20 spectrophotometer from PerkinElmer. The protein content was determined by referencing a standard curve constructed using Bovine Serum Albumin (BSA).

2.7. Particle size, polydispersity index (PDI) and zeta potential measurements

The particle size, PDI, and zeta potential of the conjugates were analyzed according to the method of Sun and Zhong (2021). Each sample was diluted to 1 mg/mL and loaded into the cuvette (PCS8501), and then measured by Nano ZS Zetasizer instrument (Malvern Instruments, Worcestershire, UK), outfitted with a 4 mW He–Ne ion laser emitting at a wavelength of 633 nm. The refractive indices used for protein and aqueous phase were 1.45 and 1.33, respectively.

2.8. Determination of the secondary structure

The secondary structures of protein and conjugate samples were characterized in accordance with previously established methods (Xu et al., 2020). Samples were diluted to a concentration of 50 μg/mL and introduced into a quartz cell with a 0.1-cm optical path length. A spectropolarimeter (Chirascan, Applied Photophysics Ltd., Leatherhead, UK) was employed to quantify molecular ellipticity across a wavelength spectrum of 200–260 nm at a scan rate of 100 nm/min. The secondary structure composition was subsequently determined utilizing Circular Dichroism Neural Network (CDNN) software (Applied Photophysics Ltd.).

2.9. Surface hydrophobicity

The surface hydrophobicity of the samples was quantified employing 8-Anilino-1-naphthalenesulfonic acid (ANS), in accordance with a modified methodology previously delineated by Jiang et al. (2023). A 15-mM ANS solution (20 μL, pH 7.0) was introduced into 4 mL of sample solution (1 mg/mL) and thoroughly mixed. Following a 20-minute incubation period at ambient temperature, fluorescence measurements were conducted using a fluorescence spectrophotometer (F-7000; Hitachi Corp., Japan). The excitation wavelength was fixed at 380 nm, and emission spectra were recorded over the wavelength interval of 410–570 nm. Surface hydrophobicity (H_0) was calculated based on the slope of fluorescence intensity in relation to protein concentration.

2.10. Reactive sulfhydryl groups (R–SH)

The thiol group content (R–SH) in the samples was assessed according to a modified version of the method initially presented by Wang et al. (2019). Each sample was diluted to a concentration of 1 mg/mL and mixed with a 10 mM 5,5′-Dithiobis (2-nitrobenzoic acid) (DTNB) solution (20 μL, pH 7.0). Following a 20-minute incubation period, the absorbance of the resulting mixtures was quantified at a wavelength of 412 nm using a Lambda 20 spectrophotometer (PerkinElmer). The R–SH content was then calculated based on the molar extinction coefficient (13,600).

2.11. Fluorescence spectrometry

The fluorescence spectra of the samples were acquired based on a modified protocol, initially described in a prior study (Li et al., 2024). Each sample was dissolved to achieve a concentration of 0.2 mg/mL. Fluorescence measurements were conducted utilizing a Cary Eclipse fluorescence spectrophotometer (Varian Inc., Palo Alto, CA, USA). The excitation wavelength was designated at 280 nm, and emission spectra were collected over a range of 300–450 nm.

2.12. Antioxidant ability

The activity of 1,1-Diphenyl-2-picryl-hydrazyl (DPPH) radical scavenging was quantified based on a modified protocol (Cheng et al., 2023). Briefly, a 2 mL conjugate sample (0.1 %, w/v) was mixed with a 2 mL DPPH solution in ethanol, followed by incubating at room temperature

in the dark for 30 min. The resultant mixture was agitated at 20 °C in the absence of light for a 30-minute period using a thermo-mixer (Eppendorf, Hamburg, Germany). The mixture of sample and ethanol without DPPH solution was used as color control and ethanol solution was used as blank control. The absorbance values of these samples were then detected at 517 nm. The percentage of DPPH radicals scavenged was calculated in equation (1) as follow:

$$\text{DPPH radical scavenging activity } (\%) = \left(1 - \frac{A_s - A_b}{A_c}\right) \times 100\% \quad (1)$$

where A_b is the absorbance of color control; A_s is the sample absorbance and A_c is the blank control absorbance.

The ferric reducing ability was measured using the slightly modified procedure of Cheng et al. (2023). A 1 mL potassium ferricyanide solution (1 %, w/v) and 2 mL conjugate samples (0.1 %, w/v) were combined. The resulting mixture was incubated in a 50 °C water bath for 20 min. Subsequently, a 1 mL trichloroacetic acid solution (10 %, w/v) was introduced to the mixture and then a 1 mL aliquot of this solution was then mixed with 3 mL of deionized water and 0.4 mL ferric chloride solution (0.1 %, w/v). This resultant mixture was allowed to react at ambient temperature for a period of 5 min. The iron reduction ability was quantified by measuring the absorbance at a wavelength of 700 nm.

2.13. Preparation of oil-in-water emulsions

A solution (80 mL) containing 5 mg/mL conjugate was homogeneously combined with fish oil (20 mL) in a volumetric ratio of 4:1. Sodium azide (NaN_3) at a concentration of 0.05 % was incorporated into the solution to inhibit microbial proliferation. This mixture was then emulsified for a duration of 3 min utilizing an UltraTurrax blender (Model KAT18, manufactured by IKA-Werke GmbH & Co. KG, Germany) operating at a speed of 16,099×*g*. Following homogenization, a 5-mL aliquot of the freshly prepared emulsion was decanted into a glass tube, which was subsequently sealed using a black plastic cap.

2.14. Emulsion morphology and stabilities

2.14.1. Morphology

An Olympus CKX53 optical microscope (Olympus Corp., Tokyo, Japan) was applied to observe the morphology of the emulsions under 400x magnification. The test emulsion was put on glass slides and covered with cover slips. On the top of cover slips, a drop of cedar wood oil was added. All the micrographs of magnified emulsions were acquired and analyzed with the software Axio Vision Rel. 4.8 (Carl Zeiss MicroImaging, GmbH, Jena, Germany) installed on a computer.

2.14.2. Creaming stability

The creaming stability of the emulsions was assessed utilizing a LUMiSizer centrifugal instrument (manufactured by L.U.M. GmbH, Berlin, Germany). This instrument expedited the rate of phase separation under an intensified gravitational field. The measurement conditions were established as follows: a centrifugal force of 3500×*g* was applied, the temperature was consistently held at 4 °C, and measurements were taken at 30-second intervals for 270 min.

2.14.3. Oxidative stability

The peroxide value (POV) and 2-thiobarbituric acid-reactive substances (TBARS) of the emulsions were determined to evaluate the oxidative stabilities when they were stored for 0, 3, 6, 9 and 12 days. POV content of the emulsions was measured using a method according to Hu et al. (2020) with some modifications. In brief, 0.3 mL emulsion was combined with 1.5 mL of isooctane/isopropanol (2:1, v/v), which was vortexed for 30 s and centrifuged at 3500 rpm for 6 min. Then 0.2 mL of the supernatant was added to 2.8 mL of a methanol/1-buthanol solution (2:1, v/v), followed by adding 20 μL of 3.94 M potassium thiocyanate and 20 μL of ferrous iron solution (made by mixing equal amounts of 0.132 M $BaCl_2$ and 0.144 M $FeSO_4$). After Fe^{2+} addition, absorbance was determined at 510 nm after incubation at room temperature for 25 min. Hydroperoxide concentrations were calculated using a standard calibration curve prepared with Fe^{3+}, which was constructed using a standard solution of an iron (III) chloride (10 μg/mL Fe).

The 2-thiobarbituric acid reactive substances (TBARS) value was determined adhering to the methodology delineated by Zhao et al. (2021). Specifically, a 2 mL aliquot of the emulsion was combined with 4 mL of a thiobarbituric acid (TBA) reagent, which consisted of 0.375 % (w/v) thiobarbituric acid and 5 % (w/v) trichloroacetic acid in a 0.25 mol/L HCl solution. This mixture was subsequently subjected to boiling at 100 °C for a duration of 30 min and was then allowed to cool to an ambient temperature of 25 °C. Following this, the solution was centrifuged at a rate of 1500 rpm and a temperature of 4 °C for 10 min. The clarified fraction was then passed through a 0.45 μm filter (Model 44525-PS, manufactured by Thermo Scientific, China), and the absorbance of the supernatant was evaluated at a wavelength of 532 nm.

2.14.4. Storage stability

The Mastersizer S3500 (Microtrac, USA) was utilized to measure the particle size distribution and ascertain the mean size of the emulsion. Subsequent to preparation, the emulsions were poured into glass containers and subjected to incubation at 4 °C for intervals of 0, 3, 6, and 12 days. Post-storage, the experimental emulsion droplet size was evaluated. The refractive index assigned to the droplet particles was 1.520, while the continuous phase was defined with a refractive index of 1.333. Prior to analysis, the emulsion sample was allowed to equilibrate for a period of 2 min within the static light scattering apparatus, maintaining a laser obscuration level of 10 %. The volume-weighted mean diameter, denoted as $d_{4,3}$, was calculated by equation (2) as follows:

$$d_{4,3} = \sum n_i d_i^4 / \sum n_i d_i^3 \quad (2)$$

where n_i was the number of droplets with diameter d_i.

2.15. Statistical analysis

All experimental procedures were conducted in triplicate. The results were presented as mean values ± standard deviations. To determine statistical differences between samples, a one-way analysis of variance (ANOVA) was employed, followed by Turkey's multiple range test, utilizing the Minitab Statistical Software. A p-value of less than 0.05 denotes statistical significance.

3. Results and discussion

3.1. Determination of CA contents of myosin-CA conjugates

As shown in Fig. 1a, CA could be effectively bound to myosin as it possessed many active phenolic hydroxyl groups and catechol moiety. The conjugates prepared with the assistance of ultrasound and microwave had higher CA binding efficiency than that of conventional method. Also, a much shorter time (30 min) was needed for the grafting process compared to that of 12 h for conventional method. Ultrasonic cavitation and electromagnetic effect led to more extensive unfolding of myosin than conventional method, thus, the active protein residues tended to be exposed for more accessible to CA. Moreover, ultrasound seemed to play a more efficient role in myosin modification as the U-myosin-CA conjugate showed higher polyphenol content (53.52 μmol/g protein) than that of M-myosin-CA conjugate (37.28 μmol/g protein). Microwave-induced overheating effect might promote protein re-aggregation before it completely unfolded, which reduced the collision chances between CA and active groups of myosin. Combined UM treatment further increased CA content within myosin-CA conjugate (80.26 μmol/g protein). It could be explained by that electromagnetic

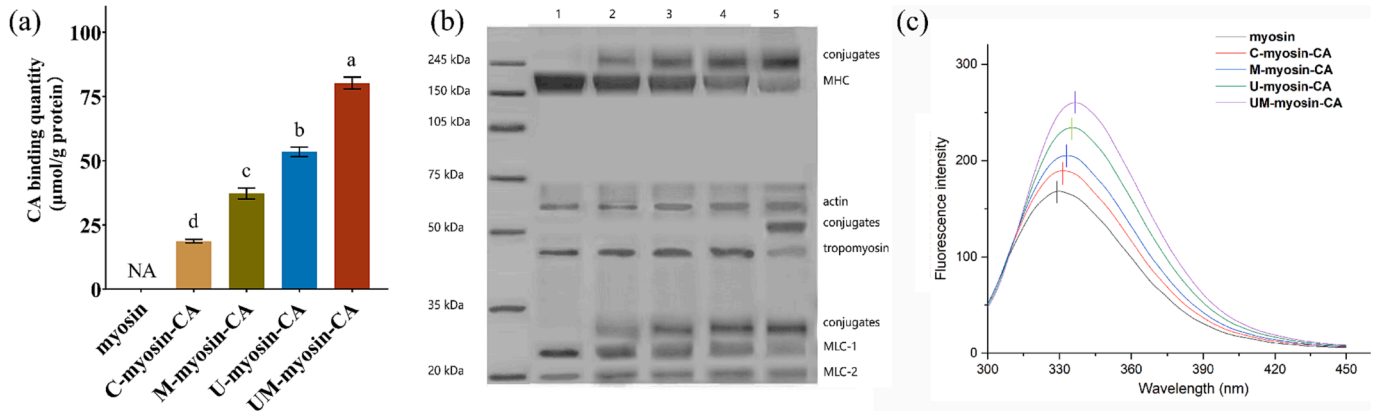

Fig. 1. (a) The quantity of chlorogenic acid (CA) grafting onto myosin; (b) the molecular weight distribution of myosin and conjugates. Column 1: myosin, Column 2: C-myosin-CA, Column 3: M-myosin-CA, Column 4: U-myosin-CA, Column 5: UM-myosin-CA; (c) the fluorescence emission spectra of myosin and conjugate. C-, M-, U-, UM- denotes to conventional method, microwave, ultrasound and combined ultrasound & microwave, respectively. Groups that do not share the same letter indicate significant difference ($p < 0.05$).

radiation smoothly unfolded the dense protein regions that were hardly available for ultrasonic mechanics; meanwhile, continual cavitation and high-frequency shear forces contributed to dissipating the local overheating. As a result, this synergistic interplay between electromagnetic radiation and ultrasonic forces promoted an optimal protein conformation, thereby enhancing the efficiency of the conjugation process.

3.2. SDS-PAGE pattern of myosin-CA conjugates

To monitor the molecular weight changes after grafting, the SDS-PAGE analysis of myosin and resultant conjugates were carried out and illustrated in Fig. 1b. Native myosin exhibited five bands for main molecular weight at about 235 kDa, 67 kDa, 46 kDa, 25 kDa and 18 kDa, which referred to myosin heavy chain (MHC), actin, tropomyosin, myosin light chain-1 (MLC-1) and myosin light chain-2 (MLC-2), respectively. New bands at approximately 250 kDa and 32 kDa were observed after myosin was conjugated with CA, while a decrease in the intensity of MHC and MLC-1 was observed, implying that CA was mainly bound with MHC and MLC-1. Given that noncovalent interactions, such as hydrophobic, hydrogen bonding, and electrostatic interactions, as well as disulfide bonds, would be disrupted by the denaturing conditions of SDS and mercaptoethanol, the retention of the structural integrity of conjugates indicated that CA was assuredly attached to the myosin through covalent bonding.

Moreover, these effects were enhanced with the assistance of microwave, ultrasound and combined UM fields. Herein, the relatively weak grafting efficiency of microwave-treated sample was mainly ascribed to that the rapid increase in temperature and strong electromagnetic radiation caused the re-folding of denatured polypeptides before it was completely conjugated (Li et al., 2020). Furthermore, the presence of 55 kDa bands were observed for UM-myosin-CA with the great shallowing of tropomyosin band. It was suggested tropomyosin structures was so strong that could not be distinctly loosened under ultrasonic treatment while coupling with microwave field would effectively weaken these structures, where compact intramolecular interactions were broken and replaced by protein–polyphenol interactions.

3.3. Solubility, particle size and zeta potential

As delineated in Table 1, native myosin exhibited a solubility of merely 25.65 %. The solubility escalated to 73.16 % upon CA grafting facilitated by the UM technique, which is likely attributable to its elevated grafting efficiency of hydrophilic CA (80.26 μmol/g myosin). Similar trends were observed in particle size distributions: the size of

Table 1
Solubility, zeta potential, particle size and poly-dispersion index (PDI) of myosin and chlorogenic acid (CA) grafted conjugates.

Samples	Solubility (%)	Particle size (nm)	PDI	Zeta potential (mV)
myosin	25.65 ± 3.79^{d}	206.81 ± 18.07^{a}	0.87 ± 0.07^{a}	−18.17 ± 1.52^{d}
C-myosin-CA	42.19 ± 5.34^{c}	128.77 ± 16.35^{b}	0.68 ± 0.03^{b}	−22.54 ± 1.15^{c}
M-myosin-CA	47.70 ± 4.66^{c}	95.87 ± 5.28^{c}	0.61 ± 0.05^{c}	−26.67 ± 0.46^{b}
U-myosin-CA	62.09 ± 2.4^{b}	51.64 ± 7.34^{d}	0.50 ± 0.01 ^{cd}	−32.30 ± 0.79^{ab}
UM-myosin-CA	73.16 ± 2.93^{a}	42.86 ± 4.91^{e}	0.46 ± 0.03^{d}	−35.98 ± 0.63^{a}

Note: All the data are expressed as mean ± standard deviation. Groups that do not share the same letter indicate significant difference ($p < 0.05$). C-, M-, U-, UM- denotes to conventional method, microwave, ultrasound and combined ultrasound & microwave, respectively.

conjugate particles was significantly reduced compared to native myosin, which had a particle size of 206.81 nm. The particle sizes followed a sequential decrease, with C-myosin-CA at 128.77 nm, M-myosin-CA at 95.87 nm, U-myosin-CA at 51.64 nm, and UM-myosin-CA at 42.86 nm. It was worthwhile mentioning that native myosin in the aqueous solution actually existed in the form of aggregates due to the association of polypeptide chains (Chen et al., 2017). Thus, native myosin in aqueous solution had quite large size, where most of myosin monomers were buried in the interior of the aggregate. Therefore, the myosin monomers had very limited rotational “freedom” to unfold or extend. However, with the covalent binding of CA, the large myosin aggregates could be broken down into smaller ones with reduced particle size and promoted unfolding tendency for a more flexible conformation (Liu et al., 2017).

In relation to zeta potential (Table 1), the conjugates displayed higher absolute zeta potential when compared to native myosin. M-myosin-CA and U-myosin-CA exhibited comparable zeta potential values, suggesting these conjugate systems had an equivalent effect in electrostatic interaction with the modification of individual microwave and ultrasound treatments. However, the concurrent application of microwave and ultrasound (UM) led to a further increment in absolute zeta potential, underscoring the advantage of this combined approach for generating conjugate with smaller particle size and more favorable charge distribution. The observed phenomena can be elucidated by the continuous and rapid flowing of bubbles and liquids accelerated heat transport and dissipation, meanwhile, electromagnetic effect could

affect the dense structural region that hardly available for ultrasound. The extremely high zeta-potential of UM-myosin-CA (absolute value of 35.98 mV) indicated that electrostatic repulsion also contributed to stabilization of the conjugates (Pan et al., 2020).

3.4. Structural properties

3.4.1. Secondary structure

As shown in Table 2, conjugation with polyphenol markedly affected the secondary structure of myosin, where the α-helix and β-sheet were transformed into β-turn and random coil. The secondary structure was stabilized by different hydrogen-bonding effect; therein, the α-helix and β-sheet referred to intra-molecular and inter-molecular hydrogen bonds among surrounding polypeptide chains, respectively; β-turn were mainly contributed by weakly hydrogen-bonded networks whereas random coil were derived from unfolded conformation (Chen et al., 2014). During conjugation, the myosin structure was prone to be unfolded, in which the hydrogen-bonded networks were disassociated and recombined into a loose structure, as some strong hydrogen bonds among the neighboring amino acids were replaced by loose protein-polyphenols and protein-water hydrogen bonding networks.

The intra-molecular ordered structure (α-helix) was readily destructed from 46.81 % to 30.98 % during conjugation with assisted techniques, but the inter-molecular ordered structure (β-sheet) was promoted during C-myosin-CA conjugation (36.88 %) when compared to native myosin (32.98 %). Interestingly, the application of ultrasound and UM resulted in much lower β-sheet values (27.88 % and 23.91 % respectively) than native myosin. These results suggest that ultrasound exposure exhibits a more pronounced deleterious effect on the ordered β-sheet structure compared to microwave irradiation.

Regarding the β-turn and random coil structures, the conjugate prepared using a conventional method displayed notably higher levels of disordered secondary structures compared to native myosin. Particularly, when the UM technique was employed, the resulting conjugate manifested the highest degree of disordered secondary structures of all the conjugates synthesized in this research. This phenomenon can be attributed to two primary mechanisms: (1) the unfolding of the helical structure, which led to the exposure of hydrophobic residues previously encapsulated within ordered configurations; and (2) CA occupied bonding sites that are originally reserved for polypeptide chains, resulting in an increased disorder in the conformation.

3.4.2. Tertiary structure

The value of H_0 and R-SH can reflect the tertiary structure of myosin and resultant conjugates as presented in Table 2. Myosin grafted with CA under conventional method, microwave, ultrasound and UM exhibited significantly higher R-SH values than that of native myosin (Table 2), which might be due to the myosin unfolding during conjugation process made the originally buried sulfhydryl groups more accessible. Therein, U-myosin-CA and UM-myosin-CA showed higher values of R-SH than those of conventional method and microwave involved samples, indicating greater structural changes for the ultrasound-assisted conjugation. In evaluating the hydrophobicity of the conjugates, as quantified by H_0, neither the conventional method nor the microwave-assisted preparations resulted in statistically significant increases in H_0 values relative to native myosin. However, the incorporation of ultrasound during the conjugate synthesis process (as in U-myosin-CA and UM-myosin-CA) led to the profound increase in conjugate hydrophobicity. These further confirm that ultrasound is more efficacious than both conventional method and microwave methods in structural modification of myosin and orienting its hydrophobic residues toward the conjugate surface. Native myosin was prone to associate into highly aggregated protein complexes, in which most of hydrophobic components were unavailable for ANS (Chen et al., 2017). Because grafted CA was like to occupy the sites that originally stabilized H-bonds and hydrophobic interactions. Protein-protein H-bonds and hydrophobic interactions that maintained highly aggregated structures gradually continuous disengaged. Hence, the large structures were transformed into smaller forms, in which they had enough degree of freedom to expand and rotate into more unfolded conformation. In this case, the protein-water interaction was greatly improved with higher solubility.

3.5. Fluorescence analysis

The fluorescence residues within the myosin, including tryptophan (Trp), tyrosine (Tyr), and phenylalanine (Phe) residues, can produce strong fluorescence quantum yield under the excited state. The grafting with polyphenols could deeply influence the protein structure, which could be revealed by its intrinsic fluorescence spectrum as illustrated in Fig. 1c. After grafting with CA, the fluorescence intensity increased with the red-shift of the maximum absorption wavelength (λ_m), indicating fluorescence groups transformed from molecular interior and enhanced the surface hydrophobicity. Grafting with CA rearranged the intra- and inter-molecular forces, where the strong protein–protein hydrogen bonds and hydrophobic interactions tend to be disassembled and more protein-water and protein–polyphenol interactions were formed under polar environment. Extrinsic microwave and ultrasound fields improved the amount of covalent protein–polyphenol crossings, thus structural changes became more obvious than that of conventional method. When grafting CA with myosin under UM technique, the maximum λ_m with the highest fluorescence intensity was observed, suggesting there was an obvious synergy between microwave and ultrasonic field to adjust myosin into suitable conformation and further improved polyphenol conjugation.

3.6. Activities of DPPH radical scavenging and iron reduction

The influence of grafting polyphenols on antioxidative activity of various conjugates was presented in Fig. 2, in which scavenging of free radicals and binding of metal ions were selected as studied parameters. The myosin-CA conjugates demonstrated superior DPPH radical scavenging abilities compared to native myosin, with UM-myosin-CA exhibiting the most potent antioxidant capacity (Fig. 2a). It had been proved that R-SH and aromatic residues on the protein surface was mainly responsible for hydrogen donors, were critical to scavenge free radical (Peredo-Lovillo et al., 2022). In native myosin, these groups were

Table 2
The secondary and tertiary structures of myosin and chlorogenic acid (CA) grafted conjugates.

Samples	Secondary structure				Tertiary structure	
	α-helix	β-sheet	β-turn	random coil	H_0	R-SH
myosin	46.81 ± 2.87^{a}	32.98 ± 3.44^{b}	10.26 ± 0.37^{d}	9.95 ± 0.51^{d}	447.1 ± 27.87^{d}	3.22 ± 0.22^{e}
C-myosin-CA	37.66 ± 5.12^{b}	31.55 ± 1.58^{b}	14.59 ± 0.60^{b}	16.20 ± 1.29^{c}	509.88 ± 30.8^{c}	4.81 ± 0.50^{d}
M-myosin-CA	33.56 ± 1.08^{c}	36.88 ± 3.06^{a}	12.25 ± 1.08^{c}	17.31 ± 0.90^{c}	487.2 ± 23.39 ^{cd}	6.39 ± 0.36^{c}
U-myosin-CA	32.16 ± 2.10^{c}	27.88 ± 0.98^{c}	19.79 ± 0.72^{a}	20.17 ± 2.07^{b}	563.73 ± 21.90^{b}	7.21 ± 0.59^{b}
UM-myosin-CA	30.98 ± 1.38^{d}	23.91 ± 1.45^{d}	20.80 ± 1.23^{a}	24.31 ± 1.25^{a}	620.78 ± 19.60^{a}	7.72 ± 0.62^{a}

Note: All the data are expressed as mean ± standard deviation. Groups that do not share the same letter indicate significant difference ($p < 0.05$). C-, M-, U-, UM- denotes to conventional method, microwave, ultrasound and combined ultrasound & microwave, respectively.

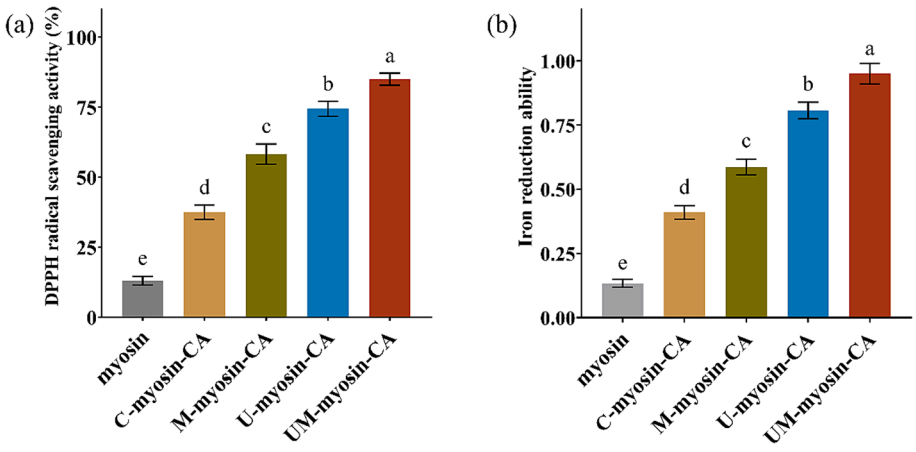

Fig. 2. Antioxidant activity of conjugates developed by myosin and chlorogenic acid (CA), (a) radical scavenging activity and (b) iron reduction ability. C-, M-, U-, UM- denotes to conventional method, microwave, ultrasound and combined ultrasound & microwave, respectively. Groups that do not share the same letter indicate significant difference ($p < 0.05$).

sequestered within the protein structure, limiting their interaction with radicals. Conjugation with CA not only enhanced the accessibility of R-SH and aromatic residues, but also incorporated reductive hydroxyl groups from polyphenolic structure, which could stabilize radical intermediates effectively (Feng et al., 2023). This dual mechanism was markedly amplified in conjugates synthesized using the UM technique.

Consistent with the DPPH assay results, U-myosin-CA and UM-myosin-CA showed superior ferric ion reducing capacities compared to other conjugates and native myosin, as depicted in Fig. 2b. The catechol domains of the grafted phenolic compounds might function as reductants, and their activity was positively correlated with the amount of polyphenol conjugated (Ipek et al., 2023). Cheng et al. (2023) also revealed that the ferric reducing ability of protein–polyphenol conjugates is significantly augmented in proportion to the polyphenol content.

3.7. Emulsions stabilized by fabricated conjugates

3.7.1. Emulsion morphology

As shown in Fig. 3a, emulsion stabilized by native myosin was found to be highly flocculated with the presence of severe aggregation. The aggregated polypeptide structures and poor amphipathic nature made them less effective in covering oil droplets. The aggregation degree of the emulsions stabilized by conjugates were decreased with the reduction of flocculation, in which more flexible conformation and higher surface hydrophobicity contributed to diffusion, absorption, and rearrangement at the interface (Pan et al., 2022). Compared to C-myosin-CA, the morphology of oil droplets became more homogeneous when emulsified by M-myosin-CA and U-myosin-CA conjugates. This could be attributed to the increase in the number of grafted polyphenols promoted the aggregation among conjugates in the O/W interface, thus contributed to a strong interfacial film against flocculation and creaming. In particular, the UM-myosin-CA conjugate developed the smallest droplet size and the most uniform emulsion system with no flocculation, and it could be considered as the most favorable emulsifier among the studied conjugates. Therefore, it was proposed that synergism between ultrasound and microwave improved the grafting efficiency of polyphenols onto myosin, leading to the most satisfactory interfacial behaviors.

3.7.2. Creaming stability

A centrifugal analyzer was utilized to simulate intense gravitational fields, in which oil droplets were accelerated to flocculate and ascend, thereby forming a creaming layer. This method effectively mimics the acceleration of droplet movement under enhanced gravitational forces, providing insights into the dynamics of emulsion stability under such conditions. Hence, the creaming process can be recorded by time- and space-dependent transmission profiles as fewer changes of the transmission and a gentle slope of the resultant curve indicated smaller degree of phase separation (Levy et al., 2021). As shown in Fig. 3b, the steep slope was observed for myosin-stabilized emulsion whereas the evolution of the transmission profiles of emulsions stabilized by myosin-CA conjugates were much less mild. The grafting of proteins with CA increased their surface hydrophobicity and induced a more flexible conformation. As a result, the resultant conjugates exhibited an enhanced propensity for precise and preferential absorption into the interfacial phase. This initial absorption facilitated the subsequent rearrangement and interaction with adjacent conjugates, leading to the formation of a compact, stable, and multi-layered film. This film effectively stabilized the emulsion, providing substantial resistance against gravity-induced creaming.

UM-myosin-CA conjugate exhibited the highest creaming stability, as the corresponding emulsion was not extensively separated after 270 min centrifugation. Compared with other conjugates, UM-myosin-CA exhibited higher solubility with more suitable conformation, which promoted conjugates to rapidly transform into intermediate structures and increase the density of resultant interfacial film. Also, the outward structure provided steric hindrance among oil droplets. Thus, the employment of UM led to the well-controlled grafting reaction between myosin and CA, and this synergistic effect endowed myosin molecules with improved interfacial behaviors under strong gravitational field.

3.7.3. Oxidation stability

PUFAs are highly susceptible to oxidation, which leads to the formation of undesirable compounds during storage (Tang et al., 2023). This oxidative process accelerates the separation in thermodynamically unstable systems, resulting in increased aggregation and uncontrollable creaming. The change of TBARs in PUFA-based emulsions was quantitatively assessed, as illustrated in Fig. 4. Following a storage period of 3 days, the TBARs concentrations were maintained at low levels, remaining below 2 μmol/L. Upon extending the storage duration to 6 days, the emulsion stabilized by myosin exhibited a TBARs concentration of 4.03 μmol/L. However, the conjugate-stabilized emulsions demonstrated stronger stability, particularly those stabilized by U-myosin-CA and UM-myosin-CA, which recorded TBARs concentrations of 1.42 μmol/L and 1.07 μmol/L, respectively. After the 9 days storage, both U-myosin-CA and UM-myosin-CA continued to outperform other conjugates. Notably, at the 12-day storage, UM-myosin-CA surpassed U-myosin-CA in stabilizing the emulsion, as reflected by its significantly lower TBARs concentration of 4.61 μmol/L compared to U-myosin-CA's

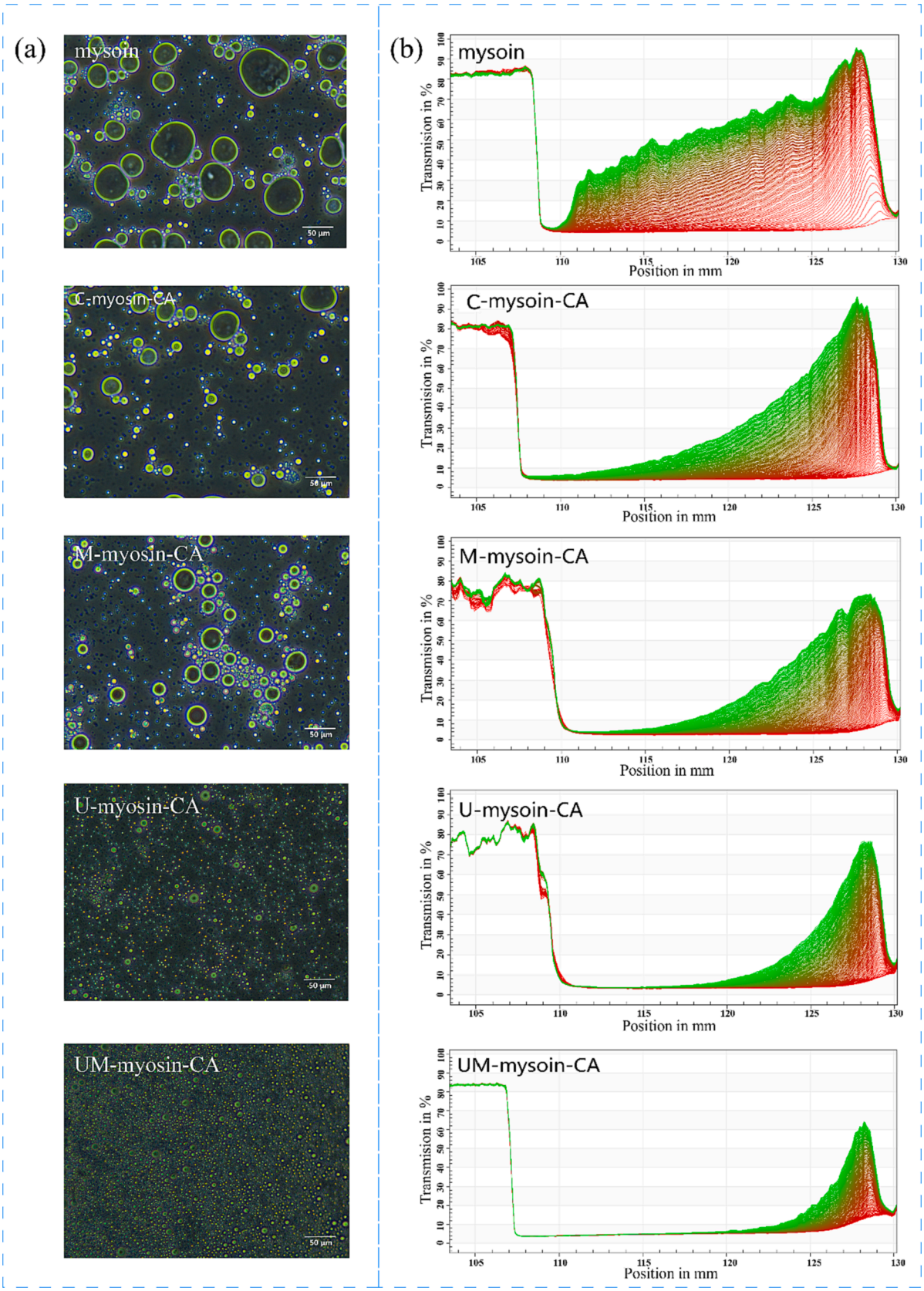

Fig. 3. (a) Optical images of emulsion stabilized by myosin and chlorogenic acid (CA) grafted conjugates different conjugates; (b) evolution of transmission profiles of emulsions stabilized by different conjugates. C-, M-, U-, UM- denotes to conventional method, microwave, ultrasound and combined ultrasound & microwave, respectively.

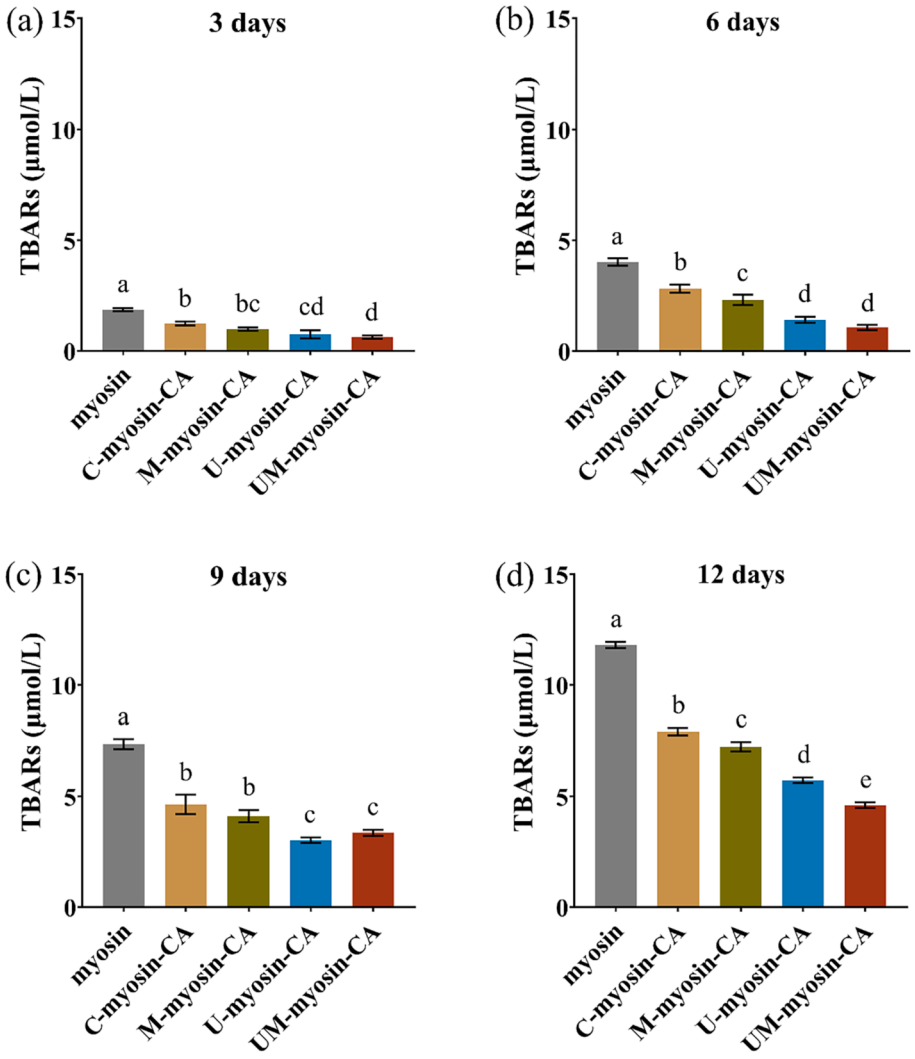

Fig. 4. The TBARS concentration of emulsions stabilized by myosin and chlorogenic acid (CA) grafted conjugates at different storage stages (a) 3 days, (b) 6 days, (c) 9 days and (d) 12 days. C-, M-, U-, UM- denotes to conventional method, microwave, ultrasound and combined ultrasound & microwave, respectively. Groups that do not share the same letter indicate significant difference ($p < 0.05$).

5.73 μmol/L.

On the one hand, the bound CA played a pivotal role in stabilizing active radicals and sequestering transition metal ions from oil droplets, thereby mitigating oxidative damage to the emulsion system under environmental stress; on the other hand, the structural configuration of UM-myosin-CA significantly shielded the diffusion of oxidizing agents. As shown in Fig. S1 of peroxide value (POV) contents, the trend observed was corroborated by the fact that emulsions stabilized with the conjugates demonstrated consistently lower POV levels compared to the emulsion stabilized with native myosin over the storage duration. Notably, the emulsion stabilized by UM-myosin-CA exhibited the greatest resistance to POV formation. The emulsion stabilized by UM-myosin-CA also exhibited high creaming stability, further suggesting that the UM-assisted grafting was an efficient method to develop high-performance myosin-based emulsifier.

3.7.4. Storage stability

The particle sizes of emulsion droplets across various storage durations were also evaluated as detailed in Table S1. Initially, the particle size of the myosin-stabilized emulsion droplet was measured at 56.73 μm. Emulsions stabilized by myosin-CA conjugates demonstrated much smaller droplet sizes. Following a storage period of 3 days, the particle size of the myosin-stabilized emulsion increased to such an extent that quantification became unfeasible. Conversely, the conjugate-stabilized emulsions maintained the stability, with UM-myosin-CA presenting the smallest droplet size at 13.14 μm. This trend persisted over storage durations of 6 and 12 days, with emulsions stabilized by UM-myosin-CA exhibiting the smallest droplet sizes among the fabricated conjugates.

Myosin is difficult to adsorb steadily in the O/W surface due to unbalanced hydrophilic/hydrophobicity portion, and the highly-folded structures limit the subsequent structural changes during emulsification (Huang et al., 2021). The covalent attachment of CA increased surface hydrophobicity of myosin; consequently, the affinity between the resulting conjugates and droplet surface was dramatically enhanced, which contributed to forming a new interface with lower interfacial energy. Besides, the unfolded conformation, reflected by fluorescence spectra, was more prone to rearrange and combine into a stable interfacial film, and it would act as a robust physical barrier protecting emulsion from phase separation. A suitable structure developed by combined UM treatment and conjugation of CA could be token as a desired module for manufacturing a well-structured emulsion system, which not only effectively compensated the interfacial behavior shortcomings of myosin but also offered a protective barrier against oxidative agents.

4. Conclusions

The present study investigated the innovative application of grafting CA onto myosin protein, utilizing a range of techniques including conventional method, ultrasound, microwave, and UM. The findings of this study highlighted the UM technique as the most proficient method, leading to a high grafting yield of 80.26 μmol/g myosin through covalent bonding, and CA was mainly bound with myosin heavy chain and myosin light chain-1, which paved the way for significant improvements in both structural and emulsifying properties of myosin-based conjugate. It was also notable that employing the assisting techniques required a much shorter time for the grafting process than the conventional method. The structural transformations induced by UM were profound, transitioning from order structures (α-helix and β-sheet) to disordered forms, thereby enhancing the amphipathic nature of the conjugates. This transition was further corroborated by fluorescence spectrometry results. Additionally, the covalent binding of CA greatly increased the capacity for radical scavenging and iron-reducing activities. Furthermore, UM-myosin-CA could be considered as an optimal emulsifying agent, capable of stabilizing emulsions against various forms of creaming, oxidative stresses, and storage. Overall, our study proved that the synergistic application of ultrasound and microwave technologies contributed to a well-performed grafting process for a significant improvement of emulsifying properties, which not only addressed the inherent interfacial behavior deficiencies of myosin but also provided a robust protective barrier against oxidative agents. This innovative approach that only required a reaction time of 30 min holds great promise for the field of food chemistry, paving the way for the development of advanced food formulations with enhanced stability and protective capabilities.

CRediT authorship contribution statement

Zhiyu Li: Visualization, Funding acquisition, Data curation, Conceptualization. **Xiaomei Zhong:** Writing – original draft, Data curation, Conceptualization. **Cuirong Luan:** Visualization, Software, Data curation. **Nanhua Wen:** Visualization, Software. **Chuanyang Shi:** Visualization, Software. **Shuji Liu:** Visualization, Conceptualization. **Yizhou Xu:** Methodology, Investigation, Conceptualization. **Quan He:** Visualization, Conceptualization. **Yijing Wu:** Conceptualization. **Jie Yang:** Writing – review & editing, Funding acquisition, Formal analysis, Conceptualization.

Declaration of competing interest

The authors declare that they have no known competing financial interests or personal relationships that could have appeared to influence the work reported in this paper.

Data availability

Data will be made available on request.

Acknowledgements

The authors gratefully acknowledge the financial support from the Natural Science Foundation of Fujian Province (No. 2023N0038, No. 2022J05242, NO. 2021J011047), Fashu Research Foundation (MFK23008), Seed Industry Innovation and Industrialization Project of Fujian Province (2021FJSCZY01) and Minjiang University.

Appendix A. Supplementary data

Supplementary data to this article can be found online at https://doi.org/10.1016/j.fochx.2024.101149.

References

Baba, W. N., McClements, D. J., & Maqsood, S. (2021). Whey protein–polyphenol conjugates and complexes: Production, characterization, and applications. *Food Chemistry, 365*, Article 130455. https://doi.org/10.1016/j.foodchem.2021.130455

Chen, X., Chen, C., Zhou, Y., Li, P., Ma, F., Nishiumi, T., & Suzuki, A. (2014). Effects of high pressure processing on the thermal gelling properties of chicken breast myosin containing κ-carrageenan. *Food Hydrocolloids, 40*, 262–272. https://doi.org/10.1016/j.foodhyd.2014.03.018

Chen, X., Tume, R. K., Xu, X., & Zhou, G. (2017). Solubilization of myofibrillar proteins in water or low ionic strength media: Classical techniques, basic principles, and novel functionalities. *Critical Reviews in Food Science and Nutrition, 57*(15), 3260–3280. https://doi.org/10.1080/10408398.2015.1110111

Cheng, J., Dudu, O. E., Zhang, J., Wang, Y., Meng, L., Wei, W., Li, X., & Yan, T. (2023). Impact of binding interaction modes between whey protein concentrate and quercetin on protein structural and functional characteristics. *Food Hydrocolloids, 142*, Article 108787. https://doi.org/10.1016/j.foodhyd.2023.108787

Feng, J., Schroën, K., Guyot, S., Gacel, A., Fogliano, V., & Berton-Carabin, C. C. (2023). Physical and oxidative stabilization of oil-in-water emulsions by roasted coffee fractions: Interface- and continuous phase-related effects. *Journal of Agricultural and Food Chemistry, 71*(11), 4717–4728. https://doi.org/10.1021/acs.jafc.2c07365

Franklin, L. M., Chapman, D. M., King, E. S., Mau, M., Huang, G., & Mitchell, A. E. (2017). Chemical and sensory characterization of oxidative changes in roasted almonds undergoing accelerated shelf life. *Journal of Agricultural and Food Chemistry, 65*(12), 2549–2563. https://doi.org/10.1021/acs.jafc.6b05357

Hauser, J., Stollberg, E., Reissmann, A., Kaunzinger, I., & Lange, K. W. (2018). Effects of omega-3 fatty acids and sugar on attention in the spontaneously hypertensive rat. *Journal of Functional Foods, 48*, 676–681. https://doi.org/10.1016/j.jff.2018.07.057

Hu, J.-N., Zheng, H., Chen, X.-X., Li, X., Xu, Y., & Xu, M.-F. (2020). Synergetic effects of whey protein isolate and naringin on physical and oxidative stability of oil-in-water emulsions. *Food Hydrocolloids, 101*, Article 105517. https://doi.org/10.1016/j.foodhyd.2019.105517

Huang, Y., Zhang, D., Zhang, Y., Fang, H., & Zhou, C. (2021). Role of ultrasound and l-lysine/l-arginine in improving the physical stability of myosin-soybean oil emulsion. *Food Hydrocolloids, 111*, Article 106367. https://doi.org/10.1016/j.foodhyd.2020.106367

Ipek, B., Artiona, L., & Decker, E. A. (2023). Synergistic mechanisms of interactions between myricetin or taxifolin with αtocopherol in oil-in-water emulsions. *Journal of Agricultural and Food Chemistry*. https://doi.org/10.1021/acs.jafc.3c01226

Iscimen, E. M., Dursun Capar, T., McClements, D. J., Yalcin, H., & Hayta, M. (2023). Ultrasound-assisted preparation of faba bean protein isolate-Vitis vinifera L. polyphenol extract conjugates: Structural and functional characterization. *Food Bioscience, 55*, Article 103041. https://doi.org/10.1016/j.fbio.2023.103041

Ji, X.-J., & Ledesma-Amaro, R. (2020). Microbial lipid biotechnology to produce polyunsaturated fatty acids. *Trends in Biotechnology, 38*(8), 832–834. https://doi.org/10.1016/j.tibtech.2020.02.003

Jiang, Z., Meng, Y., Hou, C., Gantumur, M.-A., Gao, Y., Huang, Y., Zhang, S., Sun, Y., Narantuya, S., Mu, Z., & Hou, J. (2023). Extrusion for reducing malondialdehyde-induced whey protein isolate oxidation in relation with its physicochemical, functional and intro digestive properties. *Food Hydrocolloids, 142*, Article 108730. https://doi.org/10.1016/j.foodhyd.2023.108730

Kodgire, P., Sharma, A., & Kachhwaha, S. S. (2023). Optimization and kinetics of biodiesel production of Ricinus communis oil and used cottonseed cooking oil employing synchronised 'ultrasound + microwave' and heterogeneous CaO catalyst. *Renewable Energy, 212*, 320–332. https://doi.org/10.1016/j.renene.2023.05.016

Levy, R., Okun, Z., Davidovich-Pinhas, M., & Shpigelman, A. (2021). Utilization of high-pressure homogenization of potato protein isolate for the production of dairy-free yogurt-like fermented product. *Food Hydrocolloids, 113*, Article 106442. https://doi.org/10.1016/j.foodhyd.2020.106442

Li, Z., Lin, L., Fu, G., Guo, Z., & Zhang, C. (2024). Insight on the emulsifying mechanisms of low-salt type emulsions stabilized by Maillard conjugates: Myofibrillar protein peptide-dextrin with different degrees of hydrolysis. *Food Chemistry, 433*, Article 137151. https://doi.org/10.1016/j.foodchem.2023.137151

Li, Z., Sun, Q., Zheng, Y., Wang, J., Tian, Y., Zheng, B., & Guo, Z. (2020). Effect of two-step microwave heating on the gelation properties of golden threadfin bream (Nemipterus virgatus) myosin. *Food Chemistry, 328*, Article 127104. https://doi.org/10.1016/j.foodchem.2020.127104

Li, Z., Wang, J., Zheng, B., & Guo, Z. (2020). Impact of combined ultrasound-microwave treatment on structural and functional properties of golden threadfin bream (Nemipterus virgatus) myofibrillar proteins and hydrolysates. *Ultrasonics Sonochemistry, 65*, Article 105063. https://doi.org/10.1016/j.ultsonch.2020.105063

Liu, R., Liu, Q., Xiong, S., Fu, Y., & Chen, L. (2017). Effects of high intensity unltrasound on structural and physicochemical properties of myosin from silver carp. *Ultrasonics Sonochemistry, 37*, 150–157. https://doi.org/10.1016/j.ultsonch.2016.12.039

Liu, X., Xue, F., & Adhikari, B. (2023). Production of hemp protein isolate-polyphenol conjugates through ultrasound and alkali treatment methods and their characterization. *Future Foods, 7*, Article 100210. https://doi.org/10.1016/j.fufo.2022.100210

Lv, Y., Sun, X., Jia, H., Hao, R., Jan, M., Xu, X., Li, S., Dong, X., & Pan, J. (2023). Antarctic krill (Euphausia superba) oil high internal phase emulsions improved the lipid quality and gel properties of surimi gel. *Food Chemistry, 423*, Article 136352. https://doi.org/10.1016/j.foodchem.2023.136352

Nasrollahzadeh, F., Varidi, M., Koocheki, A., & Hadizadeh, F. (2017). Effect of microwave and conventional heating on structural, functional and antioxidant properties of bovine serum albumin-maltodextrin conjugates through Maillard

reaction. *Food Research International (Ottawa, Ont.), 100*(Pt 2), 289–297. https://doi.org/10.1016/j.foodres.2017.08.030

Pan, X., Fan, F., Ding, J., Li, P., Sun, X., Zhong, L., & Fang, Y. (2022). Altering functional properties of rice protein hydrolysates by covalent conjugation with chlorogenic acid. *Food Chemistry: X, 14*, Article 100352. https://doi.org/10.1016/j.fochx.2022.100352

Pan, Y., Wu, Z., Xie, Q.-T., Li, X.-M., Meng, R., Zhang, B., & Jin, Z.-Y. (2020). Insight into the stabilization mechanism of emulsions stabilized by Maillard conjugates: Protein hydrolysates-dextrin with different degree of polymerization. *Food Hydrocolloids, 99*, Article 105347. https://doi.org/10.1016/j.foodhyd.2019.105347

Peredo-Lovillo, A., Hernández-Mendoza, A., Vallejo-Cordoba, B., & Romero-Luna, H. E. (2022). Conventional and in silico approaches to select promising food-derived bioactive peptides: A review. *Food Chemistry: X, 13*, Article 100183. https://doi.org/10.1016/j.fochx.2021.100183

Sun, J., Huang, Y., Liu, T., Jing, H., Zhang, F., Obadi, M., & Xu, B. (2022). Evaluation of crossing-linking sites of egg white protein–polyphenol conjugates: Fabricated using a conventional and ultrasound-assisted free radical technique. *Food Chemistry, 386*, Article 132606. https://doi.org/10.1016/j.foodchem.2022.132606

Sun, J., Mu, Y., Mohammed, O., Dong, S., & Xu, B. (2020). Effects of single-mode microwave heating and dextran conjugation on the structure and functionality of ovalbumin–dextran conjugates. *Food Research International, 137*, Article 109468. https://doi.org/10.1016/j.foodres.2020.109468

Sun, & Zhong, Q. (2021). Alkaline conjugation of caseinate and propylene glycol alginate to prepare biopolymer complexes stabilizing oil-in-water emulsion gels. *Food Hydrocolloids, 123*, Article 107192. https://doi.org/10.1016/j.foodhyd.2021.107192

Tang, J., Zhang, B., Liu, D., Gao, K., Dai, Y., Liang, S., Cai, W., Li, Z., Guo, Z., Hu, J., Zhou, Z., Xie, M., & Hou, S. (2023). Dietary riboflavin supplementation improves meat quality, antioxidant capacity, fatty acid composition, lipidomic, volatilomic, and proteomic profiles of breast muscle in Pekin ducks. *Food Chemistry: X, 19*, Article 100799. https://doi.org/10.1016/j.fochx.2023.100799

Wang, D., Li, H., Hou, T.-Y., Zhang, Z.-J., & Li, H.-Z. (2024). Effects of conjugated interactions between Perilla seed meal proteins and different polyphenols on the structural and functional properties of proteins. *Food Chemistry, 433*, Article 137345. https://doi.org/10.1016/j.foodchem.2023.137345

Wang, J., Li, Z., Zheng, B., Zhang, Y., & Guo, Z. (2019). Effect of ultra-high pressure on the structure and gelling properties of low salt golden threadfin bream (Nemipterus virgatus) myosin. *LWT, 100*, 381–390. https://doi.org/10.1016/j.lwt.2018.10.053

Wei, Z., Yang, W., Fan, R., Yuan, F., & Gao, Y. (2015). Evaluation of structural and functional properties of protein–EGCG complexes and their ability of stabilizing a model β-carotene emulsion. *Food Hydrocolloids, 45*, 337–350. https://doi.org/10.1016/j.foodhyd.2014.12.008

Xu, Y.-T., Wang, Y.-H., Chen, F.-P., & Tang, C.-H. (2020). Whether ovalbumin performs as a particulate or polymeric emulsifier is largely determined by pH. *Food Hydrocolloids, 103*, Article 105694. https://doi.org/10.1016/j.foodhyd.2020.105694

Xue, Z., Liu, J., Li, Q., Yao, Y., Yang, Y., Ran, C., Zhang, Z., & Zhou, Z. (2023). Synthesis of lipoic acid ferulate and evaluation of its ability to preserve fish oil from oxidation during accelerated storage. *Food Chemistry: X, 19*, Article 100802. https://doi.org/10.1016/j.fochx.2023.100802

Yadav, R., Mohapatra, D., Subeesh, A., Shabeer, T. A., & Giri, S. K. (2023). Optimization of sequential ultrasound-microwave assisted extraction of polyphenols-rich concrete from tuberose flowers through modelling. *Process Biochemistry, 134*, 175–185. https://doi.org/10.1016/j.procbio.2023.09.021

Yan, S., Wang, Q., Yu, J., Li, Y., & Qi, B. (2023). Ultrasound-assisted preparation of protein–polyphenol conjugates and their structural and functional characteristics. *Ultrasonics Sonochemistry, 100*, Article 106645. https://doi.org/10.1016/j.ultsonch.2023.106645

Zhao, T., Huang, L., Luo, D., Xie, Y., Zhang, Y., Zhang, Y., Jiao, W., Su, G., & Zhao, M. (2021). Fabrication and characterization of anchovy protein hydrolysates-polyphenol conjugates with stabilizing effects on fish oil emulsion. *Food Chemistry, 351*, Article 129324. https://doi.org/10.1016/j.foodchem.2021.129324

Zheng, Y., Chen, B., Huang, X., Teng, H., Ai, C., & Chen, L. (2023). Ultrasound-assisted free radical modification on the structural and functional properties of ovalbumin-epigallocatechin gallate (EGCG) conjugates. *Ultrasonics Sonochemistry, 95*, Article 106396. https://doi.org/10.1016/j.ultsonch.2023.106396

Zhu, H., Zhang, M., Wang, P., Sun, C., Xu, W., Ma, J., Zhu, Y., & Wang, D. (2022). Exploring the regulating mechanism of heat induced gelation of myosin by binding with Mb hemin prosthetic group. *Food Chemistry, 382*, Article 132354. https://doi.org/10.1016/j.foodchem.2022.132354